C. R. Chimie 22 (2019) 483–489

Contents lists available at ScienceDirect

Comptes Rendus Chimie

www.sciencedirect.com

Account/Revue

Solid-state electrochemistry of metal cyanides

Électrochimie à l'état solide de cyanures métalliques

Masashi Okubo [a, *], Jérôme Long [b], Daniel R. Talham [c], Rodrigue Lescouëzec [d]

[a] *Department of Chemical System Engineering, School of Engineering, The University of Tokyo, Hongo 7-3-1, Bunkyo-ku, Tokyo 113-8656, Japan*
[b] *Institut Charles-Gerhardt de Montpellier, Ingénierie moléculaire et nano-objets, UMR 5253, UM CNRS–ENSM, Université de Montpellier, place Eugène-Bataillon, 34095 Montpellier, France*
[c] *Department of Chemistry, University of Florida, Gainesville, FL 32611-7200, USA*
[d] *Sorbonne Université, CNRS, Institut parisien de chimie moléculaire, IPCM, 4, place Jussieu, 75252 Paris cedex 05, France*

ARTICLE INFO

Article history:
Received 31 January 2019
Accepted 15 April 2019
Available online 17 May 2019

Keywords:
Battery
Cathode
Electrochemistry
Cyanide
Metal–organic framework
Porous coordination polymer
Prussian blue

ABSTRACT

Efficient energy storage in the form of batteries contributes to building sustainable society. As advanced batteries need positive electrode materials capable of larger capacity, higher voltage, and lower cost, it is important to search for novel electrode materials. Among various inorganic/organic materials, cyanido-bridged coordination compounds are promising candidates for battery electrodes due to their ability to undergo solid-state redox reaction associated with ion (de)intercalation. In this review, recent results about the thermodynamic and kinetic aspects of the solid-state electrochemistry of cyanido-bridged coordination compounds are summarized, providing a fundamental basis toward developing cyanide electrodes for advanced batteries.

Mots clé:
Batterie
Cathode
Électrochimie
Cyanure
Polymères de coordination poreux
Bleu de Prusse

RÉSUMÉ

Le stockage de l'énergie dans des batteries performantes est un élément clé pour le développement des énergies renouvelables et d'un modèle de société durable. Un des défis pour construire de nouvelles batteries plus performantes est le développement de matériaux d'intercalation pour cathode présentant de plus grandes capacités, de plus grands voltages et des coûts réduits. Parmi les divers matériaux organiques et inorganiques explorés, les polymères de coordination à pont cyanure sont des candidats prometteurs. Ceux ci peuvent s'oxyder et se réduire à l'état solide en (dés)intercalant des ions. Dans cette revue, quelques résultats récents sur les aspects thermodynamiques et cinétiques des propriétés électrochimiques des polymères de coordination à pont cyanure sont résumés, démontrant leur potentiel intérêt comme életcrodes dans de nouvelles batteries.

* Corresponding author.
E-mail address: m-okubo@chemsys.t.u-tokyo.ac.jp (M. Okubo).

https://doi.org/10.1016/j.crci.2019.04.005
1631-0748/

1. Introduction

Building green power grids is crucial to realize sustainable society. At present, it is difficult to balance uneven power demands and intermittent power from renewable sources. Therefore, advanced batteries need to be developed, which can increase our energy control and efficiency in power grids [1]. Although lithium-ion batteries are currently powering most portable electronics owing to their high energy density (ca. 250 Wh/kg and 600 Wh/L), substantial gaps exist for wide use in power grids, in terms of energy density, power density, cycle life, elemental abundance, and cost [2].

Focusing on the energy density, the positive and negative electrodes of a battery generally work using reversible ion (de)intercalation in host materials (H_P and H_N, where P and N denote positive and negative electrodes, respectively). The (de)intercalation reaction at the cathode can be described as follows: $H_P + A^+ + e^- \leftrightarrow A(H_P)$, where A^+ is intercalant cation such as Li^+ or Na^+. The net reaction, $H_P + A(H_N) \leftrightarrow A(H_P) + H_N$, of a full cell gives a charge/discharge voltage, E, as $(|\mu_A^N - \mu_A^P|)/F$, where μ_A is the chemical potential of A for each host, and F is the Faraday constant. The charge/discharge capacity Q is $F/(M_e^P + M_e^N)$, where M_e is the molecular weight of each host per one electron redox capacity. Therefore, the energy density per weight of both electrodes in a battery is given by $(|\mu_A^N - \mu_A^P|)/(M_e^P + M_e^N)$, and its increase needs to (1) decrease M_e^P or M_e^N to increase the capacity of an electrode, or (2) increase $|\mu_A^N - \mu_A^P|$ to raise the cell voltage. Because both μ_A and M_e are inherent to host materials, exploration for novel electrode materials is an important step toward developing advanced systems [3].

Another important issue is the power density that represents the charge/discharge rate capability of a battery. It is well known that the charge/discharge rate capability is limited by various polarizations: (1) polarization in electrodes, influenced by electronic conduction and ionic diffusion, (2) polarization at interfaces, impacted by overpotential and transport number, and (3) polarization in electrolytes, dependent on ionic conduction and ionic diffusion [4]. In particular, slow ion transport in host materials is considered as a major rate-determining step. Therefore, it is necessary to rationally design porous host materials that can exhibit fast ion transport [5].

Upon considering these requisites for the electrode materials of advanced batteries, coordination compounds are attractive, because they can exhibit (nano)porous and flexible structures, enabling reversible ion (de)intercalation. Importantly, the rational structural/electronic design of coordination networks allows us to control μ_A and M_e for high energy, or to achieve fast ion transport for high power. Presently, the best-studied coordination compounds for battery electrodes are cyanido-bridged coordination compounds in which ions diffuse within their open porous channels whereas electrons migrate through their cyanido-bridged frameworks. These two features, called mixed conductivity, enable electrochemical ion (de)intercalation (Fig. 1). After Neff [6] reported the solid-state electrochemistry of Prussian, the most famous and oldest cyanido-bridged compound, many research groups have studied the thermodynamic and kinetic aspects of the solid-state electrochemistry of cyanido-bridged coordination networks as well as their application to batteries [7–9].

In this review, we summarize the fundamental solid-state electrochemistry of cyanido-bridged coordination compounds.

2. Thermodynamic aspects

High energy density is achieved using positive electrode materials capable of dense ion storage at high voltage. For the electrode reaction of $H_P + xA^+ + xe^- \leftrightarrow A_x(H_P)$, the electrode potential, E, versus a reference electrode is expressed as

$$-FE = \mu_A(x) - \mu_A^{ref}$$

Note that μ_A^{ref} is constant. The chemical potential is expanded as

$$\mu_A(x) = \mu_{A^+}(x) + \mu_{e^-}(x)$$

where $\mu_{A^+}(x)$ and $\mu_{e^-}(x)$ are the chemical potentials of the ion and electron, respectively. The former is determined mainly by the change in the Madelung energy upon ion intercalation, whereas the latter is the Fermi energy [10]. Therefore, the electrode potential is dominated by the crystal structure and the electronic structure of the electrode material.

Most frameworks of cyanido-bridged coordination compounds are built from transition-metal or lanthanide cations M_A^{I+} bridged by cyanidometallates $[M_B(CN)_m]^{n-}$. For example, hexacyanidometallates $[M_B(CN)_6]^{n-}$ bridge M_A^{I+} to form Prussian blue analogues (PBAs), having a three-dimensional (3D) face-centered cubic structure [11,12]. PBA is frequently found in a nonstoichiometric form with the general formula $A_{1-x}M_A^{II}[M_B^{III}(CN)_6]_{1-x/3}\square_{x/3}$ (A = alkali ion, $\square$ = cyanidometallate vacancies). The presence of hexacyanidometallate vacancies ensures the electroneutrality of the coordination framework. Variations of M_A and cyanidometallates result in various, sometime lower dimensional, non-PBA-type porous frameworks [13,14]. Hence, using octacyanidometallates $[M(CN)_8]^{4-/3-}$ (M = Mo, W) generates various extended networks of different dimensionalities with either transition metals or lanthanide ions [15]. For instance, although the compound $[Mn(H_2O)][Mn(HCOO)_{2/3}(H_2O)]_{3/4}[Mo(CN)_8]\cdot H_2O$ is a 3D structure made of interconnected double-deck planes creating 2D open channels [16], the lanthanide-based $[Tb(H_2O)_5][W(CN)_8]$ compound is a 2D coordination network formed by corrugated layers with strong hydrogen bonds between coordinated water molecules that ensure the interlayer's interactions [17,18]. However, regardless of M_A and the framework, in most cases, the cyanidometallates $[M_B(CN)_m]^{n-}$ are the redox center of cyanido-bridged coordination compounds, which primarily determines $\mu_{e^-}(x)$, hence E.

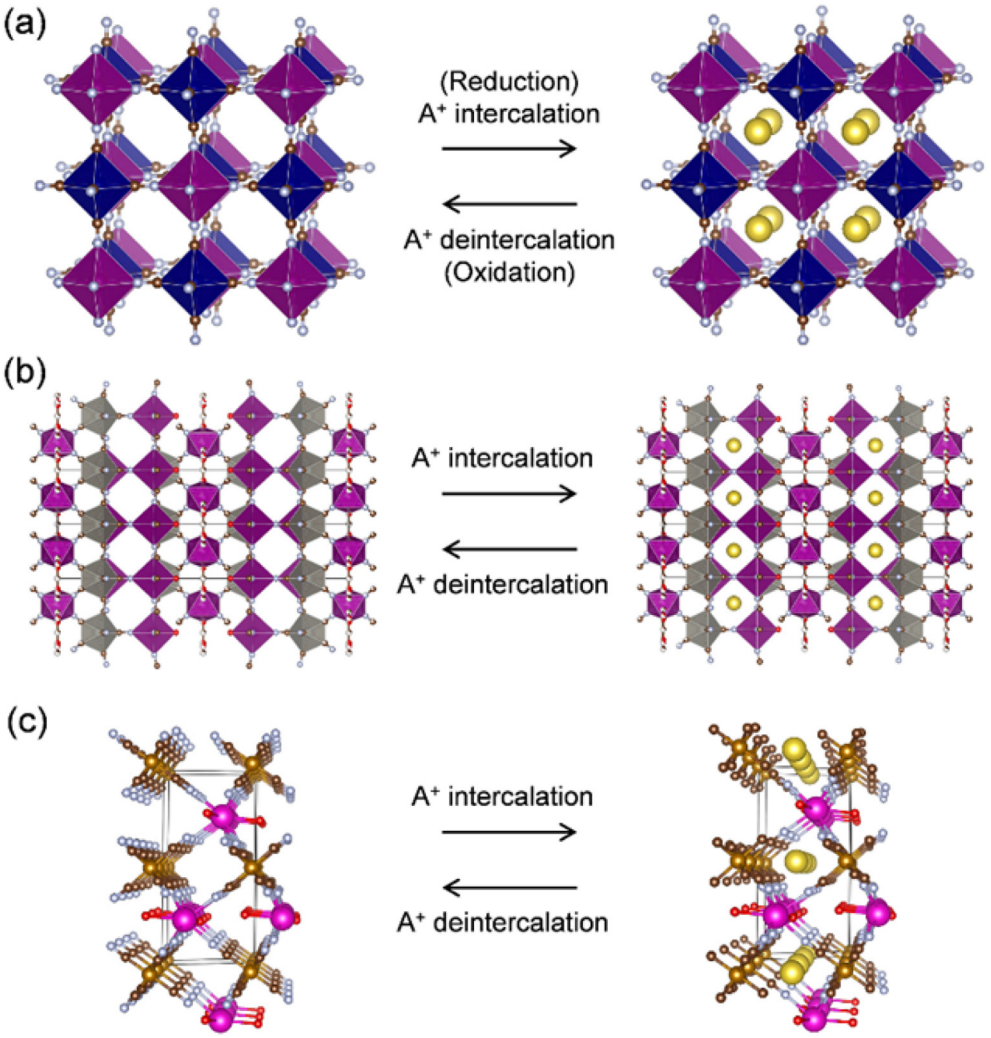

Fig. 1. Schematic illustration of ion (de)intercalation in coordination polymers: (a) Prussian blue analogue, (b) $[Mn(H_2O)][Mn(HCOO)_{2/3}(H_2O)]_{3/4}[Mo(CN)_8]\cdot H_2O$, and (c) $Eu[Fe(CN)_6]\cdot 4H_2O$.

To demonstrate the dominant role of cyanidometallates in determining *E*, Fig. 2a and b show the potential profiles of reversible Li (de)intercalation in two PBAs, $K_{0.1}Mn[Fe(CN)_6]_{0.7}\cdot\square_{0.3}\cdot 4.3H_2O$ and $K_{0.25}Ni[Fe(CN)_6]_{0.75}\cdot\square_{0.25}\cdot 5H_2O$ ($\square$ indicates a $[Fe(CN)_6]$ vacancy), in a nonaqueous Li^+ electrolyte [8,19]. Both PBAs exhibit reversible Li^+ (de)intercalation associated with the solid-state redox reaction $[Fe^{III}(CN)_6]^{3-} + e^- \leftrightarrow [Fe^{II}(CN)_6]^{4-}$. Regardless of the transition metals, Ni or Mn in the M_A site, the average reaction voltage *E* for both compounds is approximately 3.3 V versus Li/Li^+, close to the standard redox potential of $[Fe^{III}(CN)_6]^{3-}/[Fe^{II}(CN)_6]^{4-}$ (0.36 V versus standard hydrogen electrode (SHE), i.e., 3.4 V versus Li/Li^+). Fig. 2c and d show the potential profiles of Li^+ (de)intercalation for the 3D framework $[Mn(H_2O)][Mn(HCOO)_{2/3}(H_2O)_{2/3}]_{3/4}[Mo(CN)_8]\cdot H_2O$ and the bidimensional network $[Tb(H_2O)_5][W(CN)_8]$ in a nonaqueous Li^+ electrolyte [16,20]. Their average reaction voltages are approximately 3.5 and 3.4 V versus Li/Li^+, respectively, near the standard redox potentials of $[Mo^V(CN)_8]^{3-}/[Mo^{IV}(CN)_8]^{4-}$ (0.80 V versus SHE, i.e., 3.84 V versus Li/Li^+) and $[W^V(CN)_8]^{3-}/[W^{IV}(CN)_8]^{4-}$ (0.46 V versus SHE, i.e., 3.5 V versus Li/Li^+). Although the redox potential of cyanidometallates involved in the network should be modulated by the acidity of the M_A linked to the N atoms, the standard redox potential of a cyanidometallate in solution primarily governs the reaction voltage of cyanido-bridged coordination compounds. Indeed, among the hexacyanidometallates of first row transition metals Ti, Cr, Mn, Fe, and Co that can occupy the $[M_B(CN)_6]^{n-}$-site of the PBA-like networks, the standard redox potential of $[Fe^{III}(CN)_6]^{3-}/[Fe^{II}(CN)_6]^{4-}$ is the most suitable to the positive electrodes of various batteries, and most studies on the solid-state electrochemistry of cyanido-bridged coordination compounds have focused on hexacyanidoferrates [9,21,22].

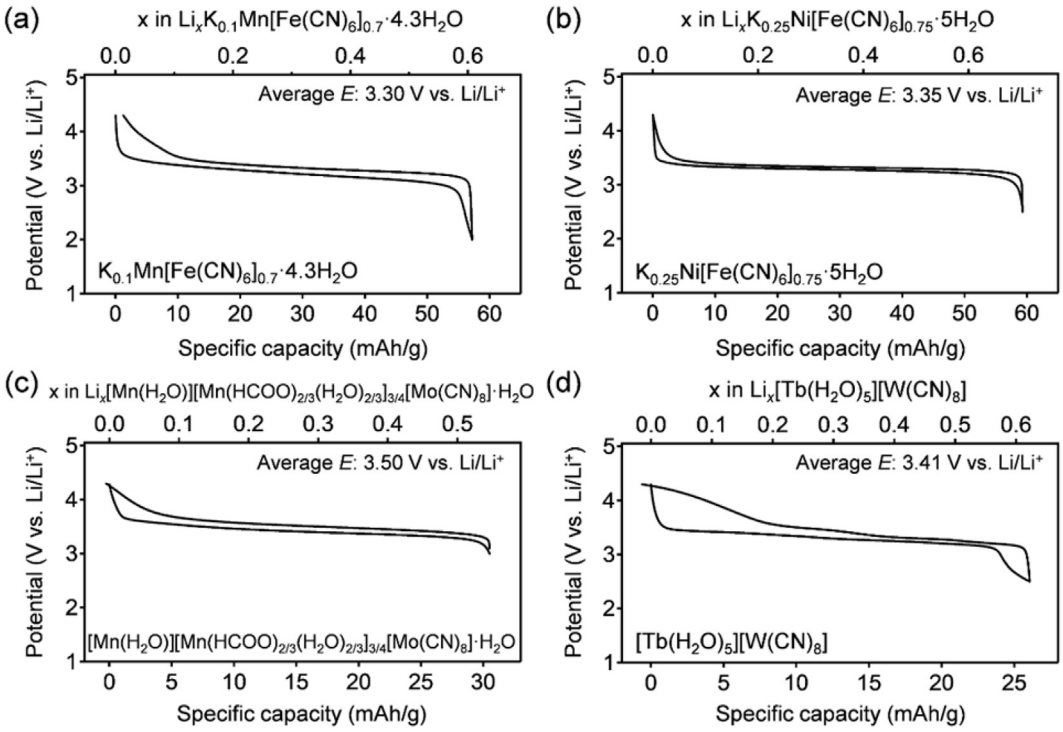

Fig. 2. Reversible Li^+ (de)intercalation potential profiles of (a) $K_{0.1}Mn[Fe(CN)_6]_{0.7}\cdot\square_{0.3}\cdot 4.3H_2O$ [8], (b) $K_{0.25}Ni[Fe(CN)_6]_{0.75}\cdot\square_{0.25}\cdot 5H_2O$ [19], (c) $[Mn(H_2O)][Mn(HCOO)_{2/3}(H_2O)]_{3/4}[Mo(CN)_8]\cdot H_2O$ [16], and (d) $[Tb(H_2O)_5][W(CN)_8]$ [20] in a 1.0 M $LiClO_4$/PC electrolyte. PC, propylene carbonate.

The electrode potential is also influenced by the chemical potential of the cation, $\mu_{A^+}(x)$. In nonaqueous electrolytes, large organic electrolyte solvents cannot be cointercalated, and desolvated A^+ is intercalated into the cyanido-bridged framework. Therefore, as an ionic radius of A^+ increases (i.e., $Li^+ < Na^+$), the ion chemical potential $\mu_{A^+}(x)$ decreases because of reduced coulombic repulsion, leading to a higher electrode potential. For example, the thin film electrode of PBA (M_A = Ni, M_B = Fe) (Fig. 3a) in nonaqueous Na^+ electrolyte exhibits a higher electrode potential than that with Li^+ electrolyte (Fig. 3b) [23,24]. On the other hand, with aqueous electrolytes, hydrated A^+ is intercalated into the framework. Although $\mu_{Li^+}(x)$ is still larger than $\mu_{Na^+}(x)$, the influence to the redox potential is not as large as in nonaqueous electrolytes, because a hydration shell screens coulombic repulsions (Fig. 3c) [23,25].

Another important aspect of the solid-state electrochemistry is the phase transformation mechanism upon ion (de)intercalation, which is generally classified into either a solid-solution or a two-phase mechanism. For the solid-solution mechanism of $H_P + xA^+ + xe^- \leftrightarrow A_x(H_P)$, A^+ and e^- are distributed homogeneously in H_p, where the concentration of A^+ changes continuously during charge/discharge. PBAs frequently exhibit a typical solid-solution reaction, which can be evidenced by the smooth shift of X-ray diffraction (XRD) peaks during charge/discharge (Fig. 4a) [19,26,27]. The linear change in lattice parameters as a function of the number of intercalated ions (Vegard's law) indicates that ion (de)intercalation occurs topochemically with preserving the host structure. On the other hand, for the two-phase mechanism of $H_P + xA^+ + xe^- \leftrightarrow x[A(H_P)] + (1 - x)[H_P]$, phase separation between $A(H_P)$ and H_P occurs, where the volume fraction of each phase changes during charge and discharge. As an example of a two-phase system, the ex situ XRD patterns for Eu$[Fe(CN)_6]\cdot 4H_2O$ show the emergence of new peaks at the expense of initial peaks upon Na^+ intercalation (Fig. 4b) [28].

For conventional electrode materials such as oxides and polyanionic compounds, the unit cell volume change by ion intercalation is considered as a descriptor of whether the reaction proceeds through the solid-solution or two-phase state [10]. Elastic repulsion between initial and final states because of the volume change increases mixing enthalpy, leading to the phase separation. However, for cyanido-bridged coordination compounds, their flexible framework can easily accommodate intercalated ions through the rotation of cyanidometallates. Indeed, the volume change of the two-phase system $Eu[Fe(CN)_6]\cdot 4H_2O$ upon Na^+ intercalation is only 1.4%, which is much smaller than that for conventional two-phase systems (6.0% for $Li_{1+x}Mn_2O_4$, 6.6% for $Li_{1-x}FePO_4$, and 8.3% $Na_{3-x}V_2(PO_4)_3$) [28]. Most likely, cooperative rotation of cyanidometallates induces the phase separation in sodiated $Eu[Fe(CN)_6]\cdot 4H_2O$. Therefore, to tailor electrochemical properties of cyanido-bridged coordination compounds, a careful structural investigation is needed.

It is also important to note that structural changes within the cyanido-bridged coordination compound electrodes are strongly influenced by the dimensionality of their framework. For example, 3D frameworks such as PBAs or $[Mn(H_2O)][Mn(HCOO)_{2/3}(H_2O)_{2/3}]_{3/4}[Mo(CN)_8]\cdot H_2O$ do

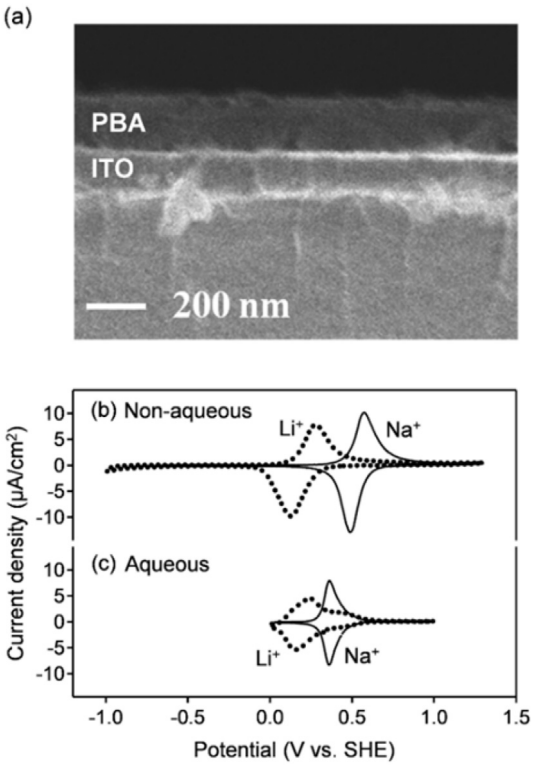

Fig. 3. (a) Scanning electron microscope image of the thin film electrode of PBA (M_A = Ni, M_B = Fe). Cyclic voltammetry (CV) curves at the scan rate of 1.0 mV/s with (b) nonaqueous Li^+ and Na^+ electrolytes, and (c) aqueous Li^+ and Na^+ electrolytes [23]. Solid and dotted lines are CV curves with Li^+ and Na^+ electrolytes, respectively.

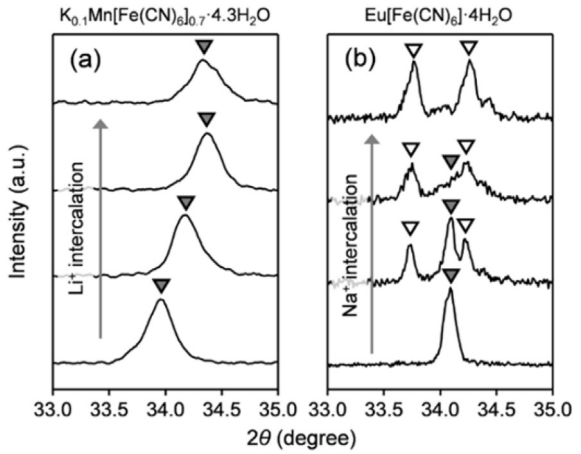

Fig. 4. Ex situ XRD patterns of (a) solid-solution system $K_{0.1}Mn[Fe(CN)_6]_{0.7}\cdot\square_{0.3}\cdot 4.3H_2O$ upon 0.7 Li^+ intercalation [8], and (b) two-phase system $Eu[Fe(CN)_6]\cdot 4H_2O$ upon 1.0 Na^+ intercalation [28].

not lose its crystallinity upon ion (de)intercalation (Fig. 5a) [16]. On the other hand, lithiation induces disorder and/or defects in the crystal networks of $[Tb(H_2O)_5][W(CN)_8]$ layers or $[Fe(Tp)(CN)_3]_2[Ni(H_2O)_2]$ chains (Tp = hydrotrispyrazolylborate), resulting in amorphous states (Fig. 5b and c) [20,29]. However, regardless of the dimensionality,

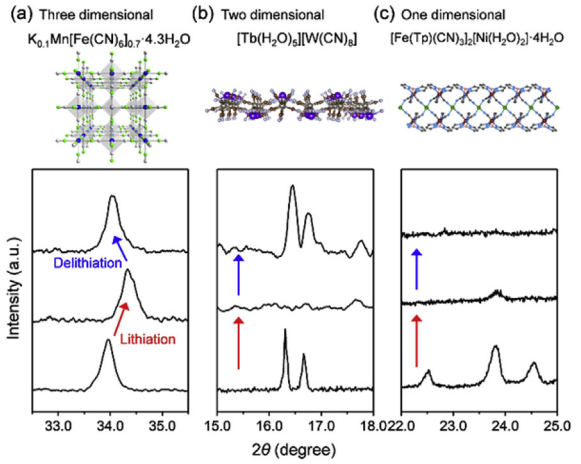

Fig. 5. Ex situ XRD patterns for (a) 3D PBA $K_{0.1}Mn[Fe(CN)_6]_{0.7}\cdot\square_{0.3}\cdot 4.3H_2O$ during 0.7 Li^+ (de)intercalation [8], (b) 2D $[Tb(H_2O)_5][W(CN)_8]$ during 1.0 Li^+ (de)intercalation [20], and (c) 1D $[Fe(Tp)(CN)_3]_2[Ni(H_2O)_2]\cdot 4H_2O$ during 2.0 Li^+ (de)intercalation [29].

the magnetic properties of the framework solids are recovered after ion intercalation and deintercalation and very close to those of an initial state, indicating that the M_B-CN-M_A links are preserved although the materials become amorphous. Therefore, the cyanido-bridged coordination networks are maintained during ion (de)intercalation even in the amorphous states.

3. Kinetic aspects

As mentioned in Section 1, the charge/discharge rate capability is limited by (1) polarization within electrodes, (2) polarization at interfaces, and (3) polarization in electrolytes. For systems that exhibit solid-solution behavior during charge and discharge, one effective way to reduce these resistances is by reducing particle size [30–32]. Although ion diffusion and electron conduction lengths become short, the large surface area of the small PBA particles reduces the areal current density and surface ion flux. Indeed, a particle size reduction of PBA (M_A = Ni, M_B = Fe) from 295 to 140 nm effectively suppresses the polarization in charge–discharge potential profiles, providing a larger capacity (Fig. 6) [33]. However, further particle-size reduction can decrease the available capacity, presumably because the number of redox-inactive sites, which may be present at the surface, increases. Therefore, it is necessary to balance the capacity and the rate capability.

In the case of the two-phase mechanism, as the charge–discharge processes are accompanied by a change in the volume fraction of each phase, the migration of phase boundaries is an important factor that predominantly limits reaction rates [34]. Large energy barriers for the boundary migration were widely reported for two-phase systems such as $Li_{1+x}Mn_2O_4$ (0.42 eV) and $Li_{1-x}FePO_4$ (0.41 eV) [32,35]. The two-phase reaction of a 3D cyanido-bridged coordination compound $Na_xEu[Fe(CN)_6]\cdot 4H_2O$ exhibits 1D boundary migration, the so-called domino cascade, where the Kolmogorov–

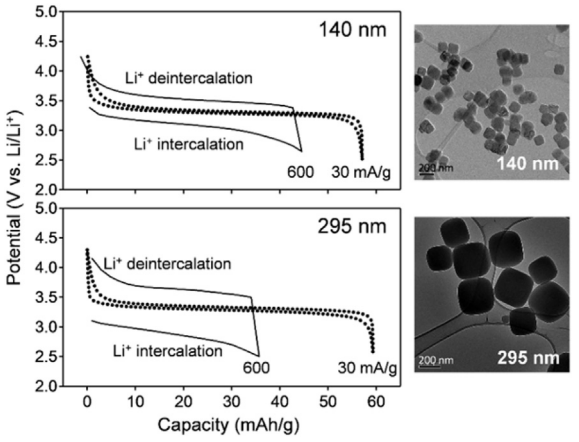

Fig. 6. Rate capability of PBA (M_A = Ni, M_B = Fe) with the average particle sizes of 140 and 295 nm, respectively [33]. Solid and dotted lines are potential profiles at the charge and discharge rates of 600 and 30 mA/g, respectively.

Johnson–Mehl–Avrami analysis revealed an energy barrier for the boundary migration as 0.11 eV [28]. This specifically small value, which was ascribed to the small volume change between sodiated and desodiated phases, indicates that the boundary migration may not be the rate-determining step in $Na_xEu[Fe(CN)_6]\cdot 4H_2O$. The kinetics of the two-phase reaction of cyanido-bridged coordination compounds is yet to be fully understood, hence further microscopic investigation on the boundary migration is needed.

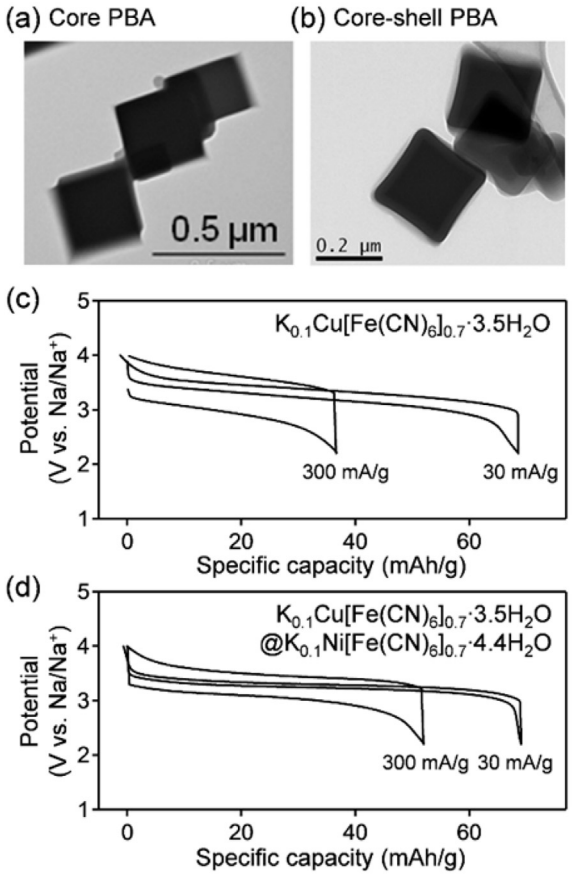

Fig. 7. TEM images of (a) core PBA (M_A = Cu, M_B = Fe) and (b) core–shell PBA (core, M_A = Cu, M_B = Fe; shell, M_A = Ni, M_B = Fe). Rate capability of (c) core PBA and (d) core–shell PBA in a nonaqueous Na^+ electrolyte [38]. Potential profiles at 300 and 30 mA/g are shown for comparison.

Reducing interfacial polarization by surface modification also improves the power density. In general, large solvated ions in organic electrolytes can penetrate the host framework only after desolvation, resulting in large energy barriers of approximately 0.5 eV for interfacial charge transfer [36]. For example, inherent surface passivation layers on PBA (M_A = Cu, M_B = Fe) decelerate interfacial charge transfer to give a poor rate capability (Fig. 7a and c) [26]. However, when the protective shell of another PBA (M_A = Ni, M_B = Fe) with lower interfacial charge–transfer resistance is deposited on the PBA (M_A = Cu, M_B = Fe), the core–shell nanoparticles enable efficient ion (de) intercalation even at high charge/discharge rates (Fig. 7b and d) [37–39]. The surface modification of cyanido-bridged coordination compounds using soft chemistry is a clear advantage over conventional electrode materials [12].

4. Conclusions

We have summarized the fundamental solid-state electrochemistry of cyanido-bridged coordination compounds. Their large electronic and structural tunability offer appealing alternatives to conventional electrode materials. From the thermodynamic point of view, the solid-state redox potential is predominantly determined by the standard redox potential of cyanidometallates in solution, albeit with a slight perturbation from ion chemical potential $\mu_{A^+}(x)$. Cyanido-bridged frameworks are robust enough to maintain the coordination network during charge and discharge. Although the loss of crystallinity can be observed in low-dimensional systems, it does not necessarily damage the intercalation properties. From the kinetic point of view, the rate capability for ion (de)intercalation can be improved by nanosizing, surface modification, and fast boundary migration. There still remain several technical concerns on the application of cyanido-bridged coordination compounds to batteries, such as their small specific and volumetric capacities (70–150 Ah/kg and 140–300 Ah/L) relative to those of oxides (150–200 Ah/kg and 750–100 Ah/L) in Li-ion cells or their lower electronic conductivities relative to those of oxides. However, they have advantages over other positive electrode materials in terms of structural/electronic designability. From the viewpoint of practical applications, as large open channels in the cyanido-bridged frameworks are suitable for the (de)intercalation of large potassium ions, their use as cathode materials for low-cost and earth-abundant potassium-ion batteries is highly promising [40]. Another possible application is aqueous batteries, where cyanido-bridged coordination compounds work as an efficient host electrode for the (de)intercalation of large hydrated monovalent, divalent, and trivalent ions [41]. Full knowledge on their solid-state electrochemistry puts forward an important prospect for electrode materials of advanced batteries.

Acknowledgments

This work was financially supported by the ANR-JST Strategic International Collaborative Research Program (SICORP), Molecular Technology, Molecular Materials for Magnesium Batteries (MoMa). M.O. and R.L. thank Michel Verdaguer for his kind intermediation to launch MoMa. J.L. thanks the University of Montpellier, CNRS, and PAC of ICGM.

References

[1] R. van Noorden, Nature 507 (2014) 26.
[2] D. Larcher, J.M. Tarascon, Nat. Chem. 7 (2015) 19.
[3] P.D. Yang, J.M. Tarascon, Nat. Mater. 11 (2012) 560.
[4] P. Simon, Y. Gogotsi, B. Dunn, Science 343 (2014) 1210.
[5] D. Sheberla, J.C. Bachman, J.S. Elias, C.J. Sun, Y. Shao-Horn, M. Dinca, Nat. Mater. 16 (2017) 220.
[6] V.D. Neff, J. Electrochem. Soc. 125 (1978) 886.
[7] N. Imanishi, T. Morikawa, J. Kondo, Y. Takeda, O. Yamamoto, N. Kinugasa, T. Yamagishi, J. Power Sources 79 (1999) 215.
[8] M. Okubo, D. Asakura, Y. Mizuno, J.D. Kim, T. Mizokawa, T. Kudo, I. Honma, J. Phys. Chem. Lett. 1 (2010) 2063.
[9] J.F. Qian, C. Wu, Y.L. Cao, Z.F. Ma, Y.H. Huang, X.P. Ai, H.X. Yang, Adv. Energy Mater. 8 (2018) 1702619.
[10] P.G. Bruce (Ed.), Solid State Electrochemistry, Cambridge University Press, Cambridge, 1995.
[11] M. Verdaguer, Chapter 2, Structure and Magnetism of Prussian Blues and Analogues: A Historical Perspective, in: G. Yannick, J. Larionova (Eds.), Prussian Blue Nanoparticles and Nanocomposites, Pan Stanford, Singapore, 2019.
[12] M.B. Zakaria, T. Chikyow, Coord. Chem. Rev. 352 (2017) 328.
[13] S. Ohkoshi, A. Namai, H. Tokoro, Coord. Chem. Rev. 380 (2019) 572.
[14] R. Lescouezec, L.M. Toma, J. Vaissermann, M. Verdaguer, F.S. Delgado, C. Ruiz-Perez, F. Lloret, M. Julve, Coord. Chem. Rev. 249 (2005) 2691.
[15] B. Sieklucka, R. Podgajny, P. Przychodzen, T. Korzeniak, Coord. Chem. Rev. 249 (2005) 2203.
[16] M. Okubo, K. Kagesawa, Y. Mizuno, D. Asakura, E. Hosono, T. Kudo, H.S. Zhou, K. Fujii, H. Uekusa, S. Nishimura, A. Yamada, A. Okazawa, N. Kojima, Inorg. Chem. 52 (2013) 3772.
[17] E. Chelebaeva, J. Larionova, Y. Guari, R.A.S. Ferreira, L.D. Carlos, F.A. Almeida Paz, A. Trifonov, C. Guérin, Inorg. Chem. 47 (2008) 775.
[18] E. Chelebaeva, J. Larionova, Y. Guari, R.A.S. Ferreira, L.D. Carlos, F.A. Almeida Paz, A. Trifonov, C. Guérin, Inorg. Chem. 48 (2009) 5983.
[19] Y. Mizuno, M. Okubo, K. Kagesawa, D. Asakura, T. Kudo, H.S. Zhou, K. Oh-ishi, A. Okazawa, N. Kojima, Inorg. Chem. 51 (2012) 10311.
[20] J. Long, D. Asakura, M. Okubo, A. Yamada, Y. Guari, J. Larionova, Inorg. Chem. 55 (2016) 7637.
[21] Y. You, X.L. Wu, Y.X. Yin, Y.G. Guo, Energy Environ. Sci. 7 (2014) 1643.
[22] K. Hurlbutt, S. Wheeler, I. Capone, M. Pasta, Joule 2 (2018) 1950.
[23] Y. Mizuno, M. Okubo, E. Hosono, T. Kudo, H.S. Zhou, K. Oh-ishi, J. Phys. Chem. C 117 (2013) 10877.
[24] Y. Mizuno, M. Okubo, D. Asakura, T. Saito, E. Hosono, Y. Saito, K. Oh-ishi, T. Kudo, H.S. Zhou, Electrochim. Acta 63 (2012) 139.
[25] Y. Mizuno, M. Okubo, E. Hosono, T. Kudo, K. Oh-ishi, A. Okazawa, N. Kojima, R. Kurono, S. Nishimura, A. Yamada, J. Mater. Chem. 1 (2013) 13055.
[26] M. Okubo, D. Asakura, Y. Mizuno, T. Kudo, H.S. Zhou, A. Okazawa, N. Kojima, K. Ikedo, T. Mizokawa, I. Honma, Angew. Chem., Int. Ed. 50 (2011) 6269.
[27] A. Flambard, A. Sugahara, S. De, M. Okubo, A. Yamada, R. Lescouëzec, Dalton Trans. 46 (2017) 6159.
[28] S. Kajiyama, Y. Mizuno, M. Okubo, R. Kurono, S. Nishimura, A. Yamada, Inorg. Chem. 53 (2014) 3141.
[29] J.R. Jimenez, A. Sugahara, M. Okubo, A. Yamada, L.M. Chamoreau, L. Lisnard, R. Lescouëzec, Chem. Commun. 54 (2018) 5189.
[30] M. Okubo, E. Hosono, J. Kim, M. Enomoto, N. Kojima, T. Kudo, H.S. Zhou, I. Honma, J. Am. Chem. Soc. 129 (2007) 7444.
[31] M. Okubo, J. Kim, T. Kudo, H.S. Zhou, I. Honma, J. Phys. Chem. C 113 (2009) 15337.
[32] M. Okubo, Y. Mizuno, H. Yamada, J. Kim, E. Hosono, H.S. Zhou, T. Kudo, I. Honma, ACS Nano 4 (2010) 741.
[33] C.H. Li, Y. Nanba, D. Asakura, M. Okubo, D.R. Talham, RSC Adv. 4 (2014) 24955.
[34] C. Delmas, M. Maccario, L. Croguennec, F. Le Cras, F. Weill, Nat. Mater. 7 (2008) 665.
[35] G. Oyama, Y. Yamada, R. Natsui, S. Nishimura, A. Yamada, J. Phys. Chem. C 116 (2012) 7306.
[36] Y. Yamada, Y. Iriyama, T. Abe, Z. Ogumi, Langmuir 25 (2009) 12766.
[37] D. Asakura, C.H. Li, Y. Mizuno, M. Okubo, H.S. Zhou, D.R. Talham, J. Am. Chem. Soc. 135 (2013) 2793.
[38] M. Okubo, C.H. Li, D.R. Talham, Chem. Commun. 50 (2014) 1353.
[39] C.H. Li, M.K. Peprah, D. Asakura, M.W. Meisel, M. Okubo, D.R. Talham, Chem. Mater. 27 (2015) 1524.
[40] J.Y. Hwang, S.T. Myung, Y.K. Sun, Adv. Funct. Mater. 28 (2018) 1802938.
[41] Z. Xing, S. Wang, A. Yu, Z. Chen, Nano Energy 50 (2018) 229.